HIGH POWER LASER
SCIENCE AND ENGINEERING

RESEARCH ARTICLE

Reducing laser beam fluence and intensity fluctuations in symmetric and asymmetric compressors

Efim Khazanov [ORCID]

Gaponov-Grekhov Institute of Applied Physics of the Russian Academy of Sciences, Nizhny Novgorod, Russia

Abstract

All space–time coupling effects arising in an asymmetric optical compressor consisting of two non-identical pairs of diffraction gratings are described analytically. In each pair, the gratings are identical and parallel to each other, whereas the distance between the gratings, the groove density and the angle of incidence are different in different pairs. It is shown that the compressor asymmetry does not affect the far-field fluence and on-axis focal intensity. The main distinctive feature of the asymmetric compressor is spatial noise lagging behind or overtaking the main pulse in proportion to the transverse wave vector. This results in a degraded contrast but reduces beam fluence fluctuations at the compressor output. Exact expressions are obtained for the spectrum of fluence fluctuations and fluence root mean square that depends only on one parameter characterizing compressor asymmetry. The efficiency of small-scale self-focusing suppression at subsequent pulse post-compression is estimated.

Keywords: self-focusing suppression; space–time overlapping; spatial and temporal self-filtering; symmetric and asymmetric compressors

1. Introduction

Present-day high-power femtosecond lasers[1] work at a fluence tens of percent lower than the laser damage threshold, as spatial noise inevitably leads to both intensity and fluence fluctuations. The spectrum of spatial noise covers scales from several wavelengths to the beam size, which is tens of centimeters in ultra-high-power lasers. The noise increasing during the propagation in a medium with cubic nonlinearity due to small-scale self-focusing, also known as the Bespalov–Talanov filamentary instability[2], plays an important role in this spectrum. The most hazardous spatial scale that leads to the so-called hot spots is of the order of 30 μm[3,4]. This noise restricts the use of post-compression after a diffraction grating compressor[4,5], as well as any other transmissive optical elements (frequency doublers, quarter-wave plates, polarizers, beam splitters). All of these elements greatly expand the applicability range of ultra-high-power lasers. To suppress filamentation instability, it is necessary to decrease the noise field intensity at the time of the maximum main pulse (maximum nonlinearity).

Even if transmissive optics are not used after the compressor, the maximum achievable energy of the output pulse is limited by the breakdown threshold of the diffraction gratings, which is especially true for the projects of 100 PW lasers proposed in China[6,7], the United States[8,9], Japan[10–12] and Russia[13] (see also the review papers[1,14]). The weakest link is the last, fourth grating, since the breakdown threshold of a femtosecond pulse is much lower than the breakdown threshold of a nanosecond pulse[15], for example, 228 versus 600 mJ/cm^2[16]. Reliable and safe operation of the compressor demands the fluence at the fourth grating to be less than the threshold with some margin. The required margin depends on fluence fluctuations. The smaller the fluctuations, the less the margin and the higher the maximum energy and laser power. Fluence fluctuations are determined by the entire spectrum of spatial noise. Note that the standard deviation of the fluence is determined by the integral of the fluctuation spectrum to which low-frequency noise makes a more significant contribution. At the same time, the magnitude of the maximum overshoot depends significantly on high-frequency noise[17].

Thus, it is highly important to reduce both the fluctuations of laser beam intensity and fluence. To do this, high-power femtosecond lasers use spatial[3,18,19] and temporal[5,20] self-filtering at free propagation in a vacuum. The term 'self-filtering' is used to emphasize that no devices are

Correspondence to: Efim Khazanov, Gaponov-Grekhov Institute of Applied Physics of the Russian Academy of Sciences, Nizhny Novgorod 603950, Russia. Email: efimkhazanov@gmail.com

required for this, only propagation in a vacuum over a certain length. Physically, self-filtering is explained by the fact that spatial noise propagates at an angle to the wave vector of the principal wave. That is why the noise lags behind the pulse of the principal wave and walks off the aperture of the principal wave beam, thus leading to temporal and spatial self-filtering, respectively. The detailed theoretical and experimental studies carried out in Refs. [21,22] showed that free space acts as a spectral filter of fluence fluctuations, with the filter transmittance being equal to the intensity autocorrelation function for spatial self-filtering and to the square of the field autocorrelation function for the temporal one.

It is obvious that the compressor, in which the beam passes a considerable distance, is also a fluence fluctuation filter, but the properties of this filter have not been studied before. Moreover, to smooth fluence fluctuations it was recently proposed to use a pair of prisms[23] and an asymmetric four-grating compressor (AFGC)[24], as well as a compressor with one pair of gratings[25,26], which is a particular case of the AFGC. Numerical simulations were carried out in Refs. [24–26] but no analytical theory was constructed.

The purpose of this paper is to provide an analytical theory aimed at quantifying the smoothing efficiency of intensity and fluence in both symmetric and asymmetric compressors and to compare self-filtering and AFGC filtering.

2. The field at the compressor output

We will consider a compressor consisting of two pairs of parallel gratings (Figure 1), on which a laser beam with an arbitrary temporal and spatial spectrum is incident. The z-axis coincides with the beam trajectory at the compressor input with $k_{x,y} = 0$ and $\omega = \omega_0 = ck_0$, where ω_0 and k_0 are, respectively, the carrier frequency and the wave vector. The angles $\alpha_{1,2}$ and $\beta_{1,2}$ of this beam are related by the grating expression as follows:

$$\sin\beta_{1,2} = m\frac{2\pi}{k_z(\omega_0)}N_{1,2} + \sin\alpha_{1,2}, \qquad (1)$$

where $N_{1,2}$ is the groove density, m is the diffraction order and $k_z^2 = k_0^2 - k_x^2 - k_y^2$. Hereinafter, the subscripts '1', '2' refer to the first and second pair of gratings, respectively. The magnitudes of α, N and L in the second pair of gratings may be either like in the first pair or different from them. In the first case, the compressor will be called a symmetric or Treacy compressor (TC)[27]. In the second case, it will be called an asymmetric compressor or AFGC[24]. The AFGC is employed in the ARC (advanced radiographic capability) picosecond laser[28,29], but asymmetry is used to make the compressor more compact, while smoothing of fluctuations is not discussed.

The ray with arbitrary k_x and ω in Figure 1 is shown by the red color. The angle of incidence on the first grating for this ray is $\alpha + \Delta\alpha(\omega, k_x)$, where $\Delta\alpha = \arctan\left(\frac{k_x}{k_z(\omega)}\right)$. The angle of the ray reflection from the grating is $\theta(\omega, k_x)$. It depends on k_x and ω, with $\theta(\omega = \omega_0, k_x = 0) = \beta$. The angles of reflection θ and β are counted to the right of the normal (i.e., for a mirror, $\beta = \alpha$). In the minus first diffraction order ($m = -1$), the angles θ and β are negative: $\beta < 0$, $\theta < 0$; therefore, the minus sign is indicated in the figure.

Let the real electric field at the compressor input at the point D1 be $\varepsilon_{in}(t,x,y) = \mathrm{Re}\{E_{in}(t,x,y)e^{i\omega_0 t - ik_0 z}\}$, where $E_{in}(t,x,y)$ is the complex amplitude. The relationship between $E_{in}(t,x,y)$ and the complex amplitude at the point D2 at the compressor output $E_{out}(t,x,y)$ is more readily found in the spectral representation. Hereinafter, the spectra
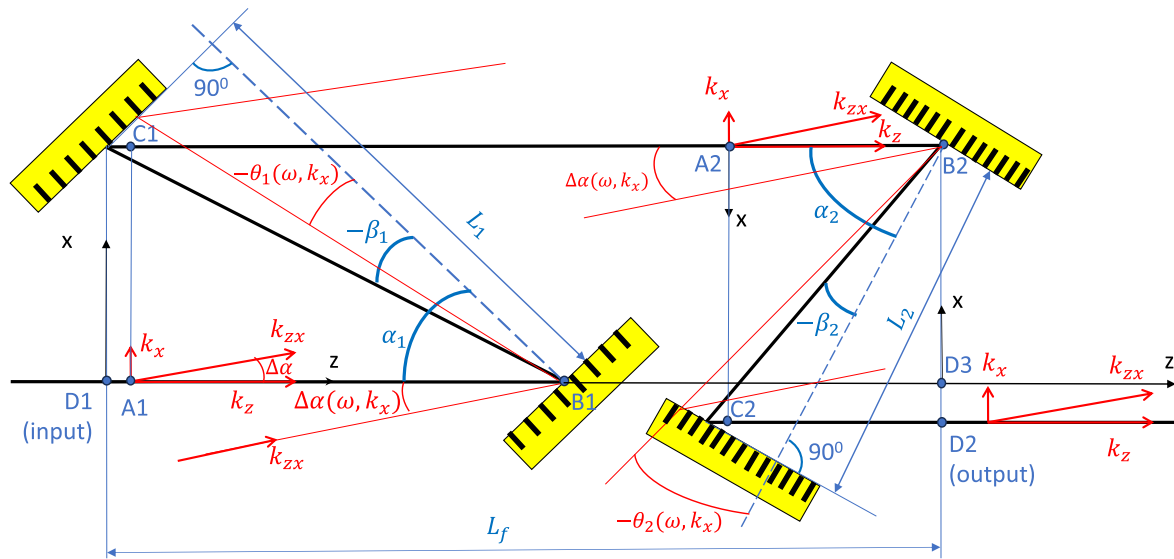

Figure 1. AFGC scheme. Gratings in each pair are parallel and identical. Distances between the gratings L, groove densities N and incidence angles α are different in different pairs.

will be designated by the same characters but with different arguments:

$$E_{\text{in, out}}(\omega, k_x, k_y) = \mathbf{F}\{E_{\text{in, out}}(t, x, y)\},$$
$$E_{\text{in, out}}(t, x, y) = \mathbf{F}^{-1}\{E_{\text{in, out}}(\omega, k_x, k_y)\}, \qquad (2)$$

where $\mathbf{F}$ and $\mathbf{F}^{-1}$ are the forward and inverse 3D Fourier transforms. Our consideration is restricted to the case of parallel and identical gratings in each pair. This ensures that the input and output wave vectors are parallel. In other words, the input and output wave vectors are always equal, and so are the frequencies. Hence, E_{out} and E_{in} are related by the following

$$E_{\text{out}}(\omega, k_x, k_y) = \exp(i\Psi(\omega, k_x, k_y)) \cdot E_{\text{in}}(\omega, k_x, k_y), \qquad (3)$$

$$E_{\text{out}}(t, x, y) = \mathbf{F}^{-1}\{\exp(i\Psi(\omega, k_x, k_y)) \cdot \mathbf{F}\{E_{\text{in}}(t, x, y)\}\}, \qquad (4)$$

where $\Psi(\omega, k_x, k_y)$ is the phase incursion between the input and output planes. For simplicity, in Equation (3) it is assumed that there are no losses and the absolute value of the transmission coefficient is equal to unity. Before passing to the expression for $\Psi(\omega, k_x, k_y)$, an important general note should be made that follows directly from Equation (3) and Parseval's theorem. The compressor changes the near-field distribution $E_{\text{out}}(\omega, k_x, k_y), E_{\text{out}}(t, k_x, k_y)$, but in no way affects the fluence in the far-field:

$$\int |E_{\text{out}}(t, k_x, k_y)|^2 dt = \int |E_{\text{in}}(t, k_x, k_y)|^2 dt.$$

This result was obtained numerically for specific examples[24,25]. We showed analytically that this statement is true for any compressor, independent of its parameters. Analogously it can be proved that the intensity on the beam axis in the far-field $|E_{\text{out}}(t, k_x = k_y = 0)|^2$ does not depend on the compressor symmetry either. The only necessary condition for this is parallel and identical gratings in each pair, otherwise Equation (3) does not hold.

The expression for $\Psi(\omega, k_x, k_y)$ (the derivation is presented in the Appendix) has the following form:

$$\Psi(\omega, k_x, k_y) = L_1 \frac{\omega}{c}\left(\cos\theta_1 + \cos\left(\alpha_1 + \frac{k_x c}{\omega}\right)\right)$$
$$+ L_2 \frac{\omega}{c}\left(\cos\theta_2 + \cos\left(\alpha_2 - \frac{k_x c}{\omega}\right)\right)$$
$$+ L_f \frac{\omega}{c} - \frac{c}{2\omega}k_x^2 L_f - \frac{c}{2\omega}k_y^2$$
$$\times \left(L_f + (\cos(\theta_1(k_{x,y} = 0)) + \cos\alpha_1)L_1 + (\cos(\theta_2(k_{x,y} = 0)) + \cos\alpha_2)L_2\right), \qquad (5)$$

where

$$\sin\theta_{1,2}(\omega, k_x, k_y) = m\frac{2\pi c}{\omega}N_{1,2}\left(1 + \frac{c^2}{2\omega^2}k_y^2\right) + \sin\left(\alpha_{1,2} \pm \frac{k_x c}{\omega}\right). \qquad (6)$$

Here, $L_{1,2}$ is the distance between the gratings along the normal and L_f is the distance between the input and output planes of the compressor (Figure 1). The first two terms in Equation (5) depend, among others, on the first power of k_x. For the TC, that is, for $L_2 = L_1$, $\alpha_2 = \alpha_1$, $N_2 = N_1$ and $\theta_2(k_x) = \theta_1(-k_x)$, this dependence disappears, while it remains for the AFGC. This is the difference between the AFGC and the TC. A compressor with a single-grating pair (single-pass single-grating pair (SSGC))[25] is a particular case of an AFGC with $L_2 = 0$.

Equation (4) with allowance for Equations (5) and (6) is sufficient for numerical simulation. To continue the analytical analysis, we will expand Equation (5) in a Taylor series.

3. Expanding $\Psi(\omega, k_x, k_y)$ in a Taylor series

By expanding Equation (5) in a Taylor series with respect to k_x, k_y and $\Omega = \omega - \omega_0$, we obtain the following:

$$\Psi(\omega, k_x, k_y) = \psi''_{x\omega}\Omega k_x + \frac{1}{2}\psi'''_{x\omega\omega}\Omega^2 k_x + \frac{1}{2}\psi''_{xx}k_x^2 + \frac{1}{2}\psi''_{yy}k_y^2$$
$$+ \frac{1}{2}\psi'''_{xx\omega}\Omega k_x^2 + \frac{1}{2}\psi'''_{yy\omega}\Omega k_y^2, \qquad (7)$$

where

$$\psi''_{x\omega} = -\frac{1}{\omega_0}(A_1 L_1 - A_2 L_2), \quad A = \frac{\cos\alpha}{\cos^3\beta}(\sin\alpha - \sin\beta), \qquad (8)$$

$$\frac{1}{2}\cdot\psi'''_{x\omega\omega} = \frac{1}{\omega_0^2}(B_1 L_1 - B_2 L_2),$$
$$B = A\left(1 - \frac{3}{2}\sin\beta\frac{\sin\alpha - \sin\beta}{\cos^2\beta}\right), \qquad (9)$$

$$\frac{1}{2}\cdot\psi''_{xx} = -\frac{c}{\omega_0}\frac{1}{2}(C_1 L_1 + C_2 L_2 + L_f),$$
$$C = \frac{\cos^2\alpha}{\cos^3\beta} - \tan\beta\sin\alpha + \cos\alpha, \qquad (10)$$

$$\frac{1}{2}\cdot\psi''_{yy} = -\frac{c}{\omega_0}\frac{1}{2}(D_1 L_1 + D_2 L_2 + L_f), \quad D = \frac{1 + \cos(\alpha + \beta)}{\cos\beta} \qquad (11)$$

$$\frac{1}{2}\cdot\psi'''_{xx\omega} = \frac{c}{\omega_0^2}\frac{1}{2}(E_1 L_1 + E_2 L_2 + L_f),$$
$$E = C + \frac{\sin\alpha - \sin\beta}{\cos^3\beta}\left(\sin\alpha - 3\sin\beta\frac{\cos^2\alpha}{\cos^2\beta}\right), \qquad (12)$$

$$\frac{1}{2}\cdot\psi'''_{yy\omega} = \frac{c}{\omega_0^2}\frac{1}{2}(F_1 L_1 + F_2 L_2 + L_f),$$
$$F = D + \frac{(\sin\beta - \sin\alpha)^2}{\cos^3\beta}, \qquad (13)$$

$$A_{1,2} = A(\alpha_{1,2}, \beta_{1,2}); \quad B, C, D, E, F - \text{analogously}. \qquad (14)$$

The lower-case letter ψ designates the values of the corresponding derivatives for $k_x = k_y = 0$ and $\omega = \omega_0$; for example:

$$\psi''_{x\omega} = \left. \frac{\partial^2 \Psi (\omega, k_x, k_y)}{\partial k_x \partial \omega} \right|_{k_{x,y} = 0; \, \omega = \omega_0} . \quad (15)$$

Some terms are omitted in Equation (7). These include terms with the first derivative with respect to k_y that are equal to zero, since Ψ depends only on k_y^2. Next, $\Psi (\omega = \omega_0, k_x = k_y = 0)$ is a constant that may also be put equal to zero. We omit $\psi'_\omega \Omega$, that is, the time delay, which does not depend on $k_{x,y}$, and $\psi'_x k_x$, that is, the Ω-independent shift along the x-axis. These terms are equivalent to the shift of the origin of the t- and x-axes, which is of no importance. Also, we omit all the terms containing derivatives only with respect to ω: $\frac{1}{2}\psi''_{\omega\omega}\Omega^2$, $\frac{1}{6}\psi'''_{\omega\omega\omega}\Omega^3$ and so on. These terms correspond to different degrees of time dispersion for a field with $k_x = 0$. In this work aimed at studying the space–time effects, we will omit the above-mentioned terms and will assume that the dispersion introduced by the compressor corresponds to the pulse dispersion at its input. Therefore, for the zero spatial frequency $k_x = 0$, the output pulse is Fourier-transform-limited. Note that for compensating higher order dispersion, the AFGC provides even more opportunities than the TC, since the AFGC has six degrees of freedom: $L_{1,2}$, $N_{1,2}$ and $\alpha_{1,2}$, whereas the TC has only three: L, N and α. Finally, we neglect all terms with derivatives with respect to $k_{x,y}$ higher than the second one, as well as all derivatives higher than the third one in view of their smallness.

Let us now address the remaining six terms in Equation (7) and the respective physical effects. The first two terms are proportional to the first power of k_x: $\psi''_{x\omega}\Omega k_x$ is the time lag by $\psi''_{x\omega}k_x$ or the shift along the x-axis by distance $\psi''_{x\omega}\Omega$; $\frac{1}{2}\psi'''_{x\omega\omega}\Omega^2 k_x$ is the pulse stretching (GVD = $\frac{1}{2}\psi'''_{x\omega\omega}k_x$) or the shift along the x-axis by distance $\frac{1}{2}\psi'''_{x\omega\omega}\Omega^2$. As seen from Equations (8) and (9), these terms in the TC are equal to zero. The second two terms in Equation (7), $\frac{1}{2}\psi''_{xx}k_x^2$ and $\frac{1}{2}\psi''_{yy}k_y^2$, correspond to diffraction that is different along the x- and y-axes, as well as to spatial self-filtering, that is, to the shift along the x- and y-axes by distance $\frac{1}{2}\psi''_{yy}k_{x,y}$. Finally, the last two terms in Equation (7) correspond to temporal self-filtering, that is, the time lag by $\frac{1}{2}\psi'''_{xx\omega,yy\omega}k_{x,y}^2$. Note that the last four terms and the corresponding effects occur not only in a compressor but also in free space. Unlike the case of the compressor, in free space they are isotropic. The expressions in parentheses for ψ in Equations (10)–(13) may be interpreted as the effective compressor length in terms of the corresponding effect. For example, $C_1 L_1 + C_2 L_2 + L_f$ is the effective length in terms of diffraction along the x-axis, and $F_1 L_1 + F_2 L_2 + L_f$ is the effective length in terms of temporal self-filtering along the y-axis. Values of the A to F constants for compressors borrowed from some works are

Table 1. Parameters of the compressors: TC[13], AFGC[24] and SSGC[25].

Parameter	TC	AFGC		SSGC
α, deg	45.5	61.0	61.0	57.0
N, 1/mm	1200	1400	1400	1400
L, mm	1850	1401	1079	2300
A	0.97	0.84	0.84	1.00
B	1.66	1.67	1.67	2.12
C	1.61	1.20	1.20	1.40
D	2.07	1.99	1.99	2.10
E	3.49	3.35	3.35	3.88
F	3.58	4.24	4.24	4.48
ΔL, mm	0	271		2303
$\Delta L'$, mm	0	539		4881

given by way of example in Table 1. Let us go into the details of these effects in different compressors.

4. The Treacy compressor as a filter of spatial frequencies

The derivatives in Equations (8) and (9) vanish in the TC, and only two effects remain in Equation (7) (spatial self-filtering and temporal self-filtering that are proportional to $k_{x,y}^2$). Thus, from the point of view of spatial effects, the TC is similar to free space, but it introduces astigmatism, because the x- and y-axes are no longer equivalent. It is seen from Equations (10) and (11) that, in terms of spatial self-filtering and diffraction, the TC supplements the free space length L_f with an additional length that is different for the x- and y-axes: $2C_1 L_1$ for the x-axis and $2D_1 L_1$ for the y-axis. With this astigmatism taken into account, the compressor is equivalent to free space with different lengths on the x- and y-axes:

$$L_{sx} = 2C_1 L_1 + L_f, \quad L_{sy} = 2D_1 L_1 + L_f. \quad (16)$$

Thus, the TC is an anisotropic transmissive filter. The transmission coefficient of such a filter can be obtained by generalizing expressions from Refs. [21,22] to the anisotropic case.

In free space, the time lag τ of the pulse propagating at an angle to the z-axis is proportional to $k_x^2 + k_y^2$. In a symmetric compressor, the coefficients of proportionality for k_x^2 and k_y^2 are not the same (see Figure 2). From Equations (12) and (13) we obtain the following:

$$\tau (k_x, k_y) = \frac{1}{2}\psi'''_{xx\omega}k_x^2 + \frac{1}{2}\psi'''_{yy\omega}k_y^2 = \frac{L_{tx}}{2c}\frac{k_x^2}{k_0^2} + \frac{L_{ty}}{2c}\frac{k_y^2}{k_0^2}, \quad (17)$$

where

$$L_{tx} = 2E_1 L_1 + L_f, \quad L_{ty} = 2F_1 L_1 + L_f. \quad (18)$$

Thus, from the point of view of temporal self-filtering, the TC adds to the free space length L_f a supplementary
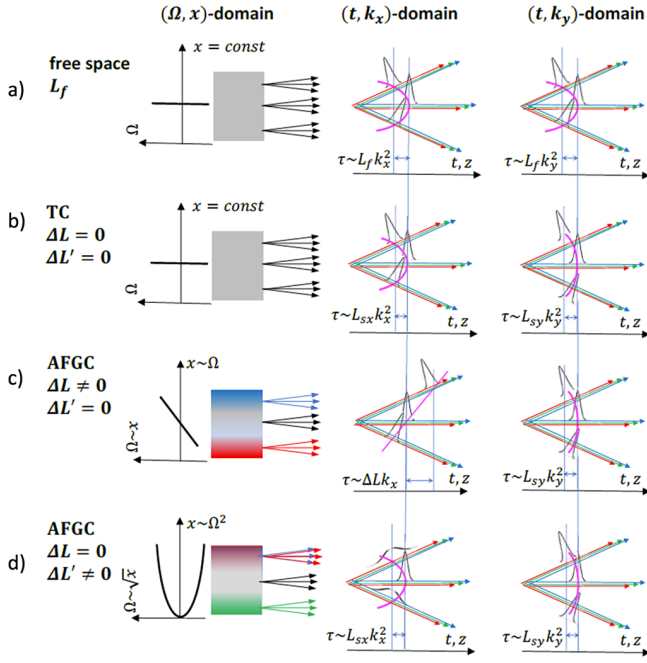
Figure 2. Schematic representation of the field after propagation in free space (a), the TC (b) and the AFGC (c), (d) in three domains. Solid magenta lines depict the intensity front.

length that is different for the x- and y-axes: $2EL$ for the x-axis and $2FL$ for the y-axis. The $L_{tx} - L_{ty}$ difference may be quite significant. Contrary to the case of free space propagation, these curvatures do not coincide after the TC. As shown in Figure 2, all other fronts are always convex because $C, D, E, F > 0$.

5. The asymmetric four-grating compressor as a filter of spatial frequencies

The effects considered in Section 4 for the TC are exactly the same as those in the AFGC. The only difference is that the effective lengths (Equations (16) and (18)) have the following form:

$$L_{sx} = C_1 L_1 + C_2 L_2 + L_f, \quad L_{sy} = C_1 L_1 + C_2 L_2 + L_f, \quad (19)$$

$$L_{tx} = E_1 L_1 + E_2 L_2 + L_f, \quad L_{ty} = F_1 L_1 + F_2 L_2 + L_f, \quad (20)$$

which directly follows from Equations (10)–(13). The most important distinctive feature of the AFGC is that Equations (8) and (9) are not zeroed, and there appear in Equation (7) two terms and, hence, two effects proportional to the first power of k_x: $\psi''_{x\omega} \Omega k_x$, that is, the time lag proportional to k_x or shift along the x-axis proportional to Ω (spatial chirp), and also $\frac{1}{2} \psi'''_{x\omega\omega} \Omega^2 k_x$, that is, GVD (pulse stretching) proportional to k_x or shift along the x-axis quadratic with respect to Ω. As seen from Equations (8) and (9), the measure of compressor

asymmetry is two parameters having the dimension of the following length:

$$\Delta L = A_1 L_1 - A_2 L_2, \quad \Delta L' = B_1 L_1 - B_2 L_2.$$

5.1. Time lag proportional to k_x or shift along the x-axis proportional to Ω: $\psi''_{x\omega} \Omega k_x$

The physical meaning of this term becomes transparent if we write $\psi''_{x\omega} \Omega k_x = X(\Omega) k_x = \tau_A(k_x) \cdot \Omega$, where $X(\Omega) = \psi''_{x\omega} \Omega$ is the beam shift along the x-axis (spatial chirp) and $\tau_A(k_x) = \psi''_{x\omega} k_x$ is the time lag. These two representations are equivalent and are illustrated in Figure 2 for clarity. From the point of view of spatial noise, this effect reduces to temporal filtering, and it is convenient to consider it in terms of the pulse time lag with $k_x \neq 0$:

$$\tau_A(k_x) = -\frac{k_x}{k_0} \cdot \frac{\Delta L}{c}. \quad (21)$$

Unlike temporal self-filtering, the time lag here is proportional to the first rather that the second (Equation (17)) power of k_x, which makes the effect much stronger. However, for $\Delta L \preccurlyeq L_x \frac{k_x}{k_0}$, the effects are comparable. The second difference is that the sign of the lag depends on the sign of k_x, that is, the spatial noise for which $k_x \Delta L > 0$ will overtake the main pulse rather than lag behind it (Figure 2). Lagging and overtaking have an identical impact on fluence smoothing. At the same time, the pulses propagating ahead of the main pulse reduce the time contrast. Note that this parasitic effect is especially strong in an SSGC. For instance, for a compressor with the parameters listed in Table 1, even large-scale (usually highly energetic) noise with $k_x = 10^{-4} k_0$ overtakes the main pulse by 0.77 ps. According to the contrary assertion made in Ref. [25], the integrated contrast does not degrade, which is evidently due to the neglect of the space–time coupling effects considered above.

It is important to note that the mentioned contrast decrease concerns only the power contrast, that is, integrally throughout the beam. From the practical point of view, contrast at the focal point is important. This contrast will not deteriorate, as the noise components overtaking the main pulse in the focal plane will be far away from the beam axis. Consequently, these components will damage the target at the beam periphery, whereas on the beam axis the target may remain intact up to the arrival of the main pulse. A quantitative study of this effect is outside the scope of this paper.

5.2. Chirp (GVD) proportional to k_x: $\psi'''_{x\omega\omega} k_x \Omega^2$

The physical meaning of this term is quite obvious – pulses with a wave vector k_x acquire, in addition to the principal

wave with $k_x = 0$, a chirp (GVD) proportional to k_x:

$$\frac{1}{2}\psi'''_{x\omega\omega}k_x\Omega^2 = \text{GVD}\,(k_x)\cdot\Omega^2 = k_x\Delta L'\cdot\frac{\Omega^2}{\omega_0^2}.$$

If the main pulse (with $k_x = 0$) at the compressor output is Fourier-transform-limited, then the noise with $k_x \neq 0$ will be extended in time independent of the sign of k_x (Figure 2). This reduces filtering caused by the noise time lag or overtaking, as stretching of the lagging or overtaking noise pulse increases its time overlap with the main pulse.

A proper choice of $L_{1,2}$, $N_{1,2}$ and $\alpha_{1,2}$ allows controlling the values of ΔL and $\Delta L'$, thus creating complex space–time distributions of the field in the focal plane. In particular, the combinations $\Delta L' = 0$, $\Delta L \neq 0$ or $\Delta L' \neq 0$, $\Delta L = 0$ demonstrated in Figure 2 can be implemented. Such distributions may be useful for charged particle acceleration or other applications. For instance, in the case depicted in Figure 2(d), the pulse duration in the focal plane at the points above and below the z-axis ($x \neq 0$) will be longer than the duration of the Fourier-transform-limited pulse on the z-axis ($x = 0$).

6. Reducing fluence fluctuations at the asymmetric four-grating compressor output

As mentioned above, all the effects proportional to the second power of $k_{x,y}$ in a TC as well as in an AFGC may be reduced to analogous effects in free space. The suppression of fluence fluctuations at free space propagation was analyzed analytically in Refs. [21,22]. These earlier results may be generalized taking into account Equations (10)–(13). Here, we will not dwell on this; instead, to clearly demonstrate the effect of compressor asymmetry, we will focus on the effects proportional to the first power of k_x, specific for the AFGC. To do this, in Equation (7) we will neglect the last four terms proportional to $k_{x,y}^2$ and leave only the first two terms. Let us compare fluence fluctuations at the AFGC output with a reference, namely a TC that is a particular case of an AFGC with $\Delta L = \Delta L' = 0$. In this case, the field $E_{\text{ref}}\,(t,x,y)$ at the TC output may be written as a sum of the main $E_0\,(x,y)\,U(t)$ and noise $E_{\text{ref,n}}\,(t,x,y)$ fields:

$$E_{\text{ref}}\,(t,x,y) = E_0\,(x,y)\,U(t) + E_0\,(x,y)\,U(t)f\,(x,y), \quad (22)$$

where $f\,(x,y)$ is a complex function and $|f\,(x,y)| \ll 1$; $\int f\,(x,y)\,\mathrm{d}S = 0$. From Equations (3) and (7)–(9) we obtain the following:

$$E_{\text{out}}\,(\omega,k_x,k_y) = E_{\text{ref}}\,(\omega,k_x,k_y)\exp\left(i\left(-\frac{\Delta L}{\omega_0}\Omega + \frac{\Delta L'}{\omega_0^2}\Omega^2\right)k_x\right). \quad (23)$$

The fluence $w_{\text{out}}\,(x,y)$ may also be represented as a sum of the main $w_{\text{out,0}}\,(x,y)$ and noise $w_{\text{out,n}}\,(x,y)$ fluences:

$$w_{\text{out}}\,(x,y) = \int |E_{\text{out}}\,(t,x,y)|^2\mathrm{d}t = w_{\text{out,0}}\,(x,y) + w_{\text{out,n}}\,(x,y). \quad (24)$$

By substituting Equations (22) and (2) into Equation (23) and the result into Equation (24) we find $w_{\text{out,n}}\,(x,y)$, from which we obtain an expression for the spectrum of fluence fluctuations $w_{\text{out,n}}\,(k_x,k_y)$:

$$\left|w_{\text{out,n}}\,(k_x,k_y)\right|^2 = T\,(k_x)\cdot\left|w_{\text{ref,n}}\,(k_x,k_y)\right|^2, \quad (25)$$

where

$$T\,(k_x) = \left|\frac{\int |U\,(\Omega)|^2\cdot\exp\left(i\left(-\frac{\Delta L}{\omega_0}\Omega + \frac{\Delta L'}{\omega_0^2}\Omega^2\right)k_x\right)\mathrm{d}\Omega}{\int |U\,(\Omega)|^2\mathrm{d}\Omega}\right|^2, \quad (26)$$

where $T\,(k_x)$ has the meaning of the spectrum filter transmittance. Two terms in the exponent correspond to two effects – lag (overtaking) and GVD. If we neglect the latter, that is, if $\frac{\Omega}{\omega_0} \ll \frac{\Delta L}{\Delta L'}$, then from Equation (26) we obtain a result fully analogous to temporal self-filtering[21,22]: the filter transmittance is equal to the square of the modulus of the autocorrelation function of the field A_t with the argument equal to the time lag τ_A (Equation (21)):

$$\left|w_{\text{out,n}}\,(k_x,k_y)\right|^2 = |A_t\,(\tau_A)|^2\cdot\left|w_{\text{ref,n}}\,(k_x,k_y)\right|^2, \quad (27)$$

where

$$A_t\,(\tau) = \frac{\int U(t)U^*\,(t-\tau)\,\mathrm{d}t}{\int |U(t)|^2\mathrm{d}t}. \quad (28)$$

The difference from the temporal self-filtering is that the time lag τ_A (Equation (21), as distinct from τ (Equation (17), is proportional to the first (rather than the second) power of k_x; besides, τ_A does not depend on k_y. As a reference noise spectrum $w_{\text{ref,n}}\,(k_x,k_y)$, we take the frequently used model[30,31]:

$$\left|w_{\text{ref,n}}\,(k_x,k_y)\right|^2 = \frac{\text{const}}{\left(h^2 + k_x^2 + k_y^2\right)^\gamma}, \quad (29)$$

where γ is a constant that takes on a value from 1 to 2 (usually 1.28), and the spatial scale $\Lambda = 2\pi/h$ is smaller but commensurable with the beam size. By integrating Equation (27) with respect to k_y, with Equation (29) taken into account, we obtain for a Gaussian pulse

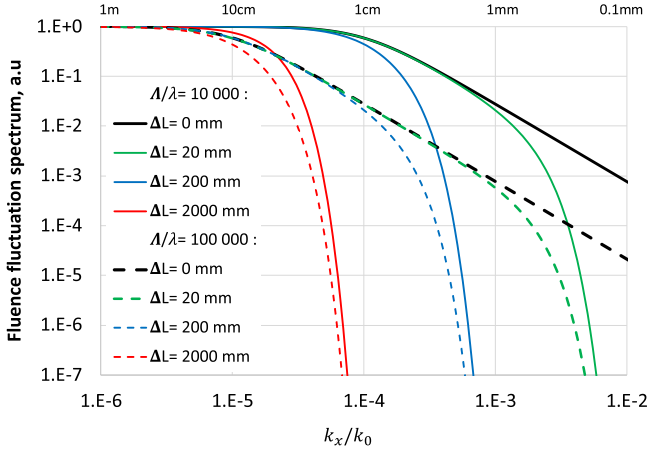**Figure 4.** Reducing the rms of fluence fluctuation $\frac{\sigma_{out}}{\sigma_{ref}}$.

Figure 3. One-dimensional fluence fluctuation spectrum $S(k_x)$ at the AFGC output for a pulse having duration $\tau_p = 30$ fs ($\gamma = 1.28$). The difference between the colored and black curves shows the efficiency of fluence smoothing at a given k_x. The efficiency of small-scale self-focusing suppression for a pulse with duration $\tau_p = 21.2$ fs will be equal to the efficiency of fluence smoothing $S(k_x)$ (see the text).

$U(t) = \exp\left(-\left(t^2/\tau_p^2\right)\right.$ a 1D spectrum:

$$S(k_x) = \int_{-\infty}^{\infty} \left|w_{\text{out, n}}\left(k_x, k_y\right)\right|^2 k_y$$

$$= \text{const} \cdot \frac{B\left(\frac{1}{2}; \gamma - \frac{1}{2}\right)}{\left(h^2 + k_x^2\right)^{\gamma - \frac{1}{2}}} \cdot \exp\left(-\left(\frac{\Delta L}{c\tau_p} \cdot \frac{k_x}{k_0}\right)^2\right),$$

(30)

where $B(a; b)$ is a B-function. The $S(k_x)$ spectrum for $\tau_p = 30$ fs is plotted in Figure 3 at different values of ΔL. Figure 3(a) clearly demonstrates filtering of high spatial frequencies in the AFGC (cf. the colored and the black curves). Knowing the fluence fluctuation spectrum $\left|w_n\left(k_x, k_y\right)\right|^2$, one can find the root mean square (rms) of the fluctuations:

$$\text{rms} = \sigma_{\text{out, ref}} = \sqrt{\int_{-\infty}^{\infty} \left|w_{\text{n; ref, out}}\left(k_x, k_y\right)\right|^2 \text{d}k_x \text{d}k_y},$$

(31)

which is a convenient quantitative characteristic of filtering efficiency: the $\sigma_{\text{out}}/\sigma_{\text{ref}}$ ratio shows how many times the fluence fluctuation rms will decrease by the AFGC compared to the TC. The substitution of Equation (30) into Equation (31) and integration with respect to dk_x yield the following:

$$\left(\frac{\sigma_{\text{out}}}{\sigma_{\text{ref}}}\right)^2 = \frac{2}{B\left(\frac{1}{2}; \gamma - 1\right)} \int_0^{\infty} \frac{\exp\left(-\left(\frac{\lambda}{\Lambda} \frac{\Delta L}{c\tau_p} \cdot x\right)^2\right)}{\left(1 + x^2\right)^{\gamma - 1/2}} \text{d}x. \quad (32)$$

For a given γ, the $\frac{\sigma_{\text{out}}}{\sigma_{\text{ref}}}$ ratio depends only on one parameter, $\frac{\lambda}{\Lambda} \frac{\Delta L}{c\tau_p}$. The corresponding dependences are plotted
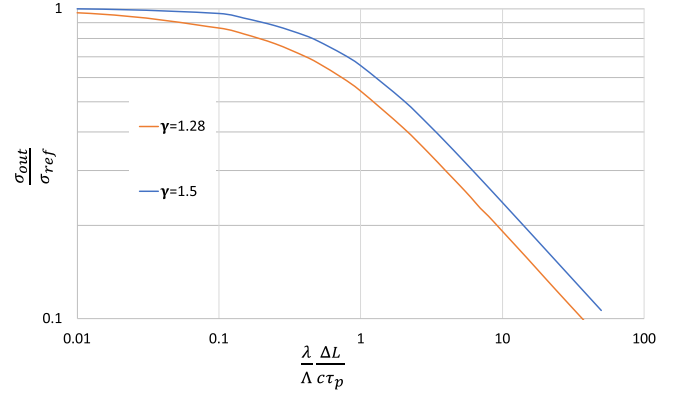
in Figure 4. One can see from the figure that the value of γ is not very important and at large $\frac{\lambda}{\Lambda} \frac{\Delta L}{c\tau_p}$ the value of $\frac{\sigma_{\text{out}}}{\sigma_{\text{ref}}}$ is proportional to $\sqrt{\frac{\lambda}{\Lambda} \frac{\Delta L}{c\tau_p}}$. Note that for beams of a smaller diameter (smaller Λ), the high-frequency components have larger values and, hence, filtering is more efficient. It is clear from Equation (32) and Figures 3 and 4 that the filtering efficiency is determined by the ratio of time $\Delta L/c$ to the pulse duration at the compressor output τ_p, which once again emphasizes the relevance of the used term 'temporal filtering'.

To conclude, we note that to find the probability for the fluence to exceed the threshold value, it is sufficient to know the fluctuation spectrum $\left|w_n\left(k_x, k_y\right)\right|^2$[17].

7. Suppressing small-scale self-focusing by means of the asymmetric four-grating compressor

Exact computation of the efficiency of small-scale self-focusing demands solution of a nonlinear nonstationary Schrödinger equation in which the field at the compressor output (Equation (4)) is used as a boundary condition at $z = 0$. This requires numerical simulation, which is outside the scope of the present work. However, the results obtained allow us to assess the efficiency of temporal filtering. For suppressing small-scale self-focusing it is necessary to reduce noise intensity I_n (rather than noise fluence) at the time of the maximum main pulse, that is, at the time of maximum nonlinearity. Consequently, the reduction of $I_{\text{out, n}}\left(t = 0, k_x, k_y\right)$ will be a good estimate. After the corresponding computations for $I_{\text{out, n}}\left(t = 0, k_x, k_y\right)$, similarly to Section 6 we will obtain an expression analogous to Equation (27):

$$I_{\text{out, n}}\left(t = 0, k_x, k_y\right) = \left|U\left(t = -\frac{k_x}{k_0} \frac{\Delta L}{c}\right)\right|^2 I_{\text{ref, n}}\left(t = 0, k_x, k_y\right).$$

(33)

Thus, from the point of view of suppressing small-scale self-focusing, an AFGC is a filter with the transmittance equal to the normalized pulse intensity at the time $-\frac{k_x}{k_0}\frac{\Delta L}{c}$. For a Gaussian pulse, $|U(t)|^2 = \left|A_t\left(t/\sqrt{2}\right)\right|^2$. Therefore, with Equations (27) and (33) taken into account, the filtering efficiency for the intensity will be the same as for the fluence shown in Figure 3, but for a $\sqrt{2}$ times shorter pulse duration, that is, 21.2 fs instead of 30 fs. As mentioned above, of primary importance is the reduction of the value of the noise intensity spectrum $I_n\left(t=0,k_x,k_y\right)$ at spatial frequencies k_{max}, for which the instability increment is the largest. For high-power femtosecond lasers, k_{max}/k_0 is of the order of 0.03[3,4], that is, as seen in Figure 3, a small compressor asymmetry ΔL is quite sufficient for effective filtering.

8. Conclusion

For reducing beam fluence fluctuations it was proposed[24] to use a compressor in which the diffraction gratings in two pairs are different, whereas all the other parameters are the same. However, this effect was investigated only numerically. In the presented paper, an analytical theory has been constructed that describes all space–time coupling effects arising in an asymmetric optical compressor, in which pairs of gratings may differ not only by the distance between the gratings but also by the groove density and angle of incidence. It has been shown that no compressor asymmetry affects the far-field fluence and on-axis focal intensity. Given that the gratings in each pair are parallel and identical, this conclusion is true for any compressor, including one with a single-grating pair.

From the point of view of beam cleanup from spatial noise, a symmetric compressor is 'similar' to free space in that it also accomplishes spatial and temporal self-filtering of a beam. The difference is that both these effects become anisotropic: the compressor is an anisotropic transmissive filter. In particular, it introduces astigmatism.

In an asymmetric compressor, there appear two additional effects proportional to the first power of the transverse wave vector, which are shown schematically in Figure 2. The spatial noise (i) lags behind/overtakes the main pulse, which is equivalent to a linear spatial chirp, and (ii) acquires a temporal chirp (GVD), which is equivalent to a squared spatial chirp. The first effect reduces beam fluence fluctuations at the compressor output. Exact expressions for the fluence fluctuation spectrum and fluence rms have been obtained, with the latter being dependent only on one parameter characterizing compressor asymmetry. The second effect reduces filtering induced by the first effect, as noise pulse stretching increases its time overlap with the main pulse. By choosing adequate grating parameters it is possible to control these two effects independently, for example, for creating complex space–time field distributions in the focal plane that may be interesting for different applications.

The asymmetric compressor is also interesting for suppressing small-scale self-focusing, for example, at subsequent post-compression. In this case, it is necessary to reduce the noise intensity rather than its fluence, which should be done at high spatial frequencies. The constructed theory made it possible to estimate the efficiency of suppression of small-scale self-focusing and showed that it may be orders of magnitude, even with a slight asymmetry of the compressor.

The disadvantages of an asymmetric compressor include the degradation of temporal contrast. The theory of this inevitable parasitic effect will be considered elsewhere.

Appendix A. Phase incursion in a compressor from point D1 to point D2

As a pulse is propagating from point A1 to point C1 (Figure 1) there occurs phase incursion:

$$\Psi_1 = L_1 k_{zx}\left(\cos\theta_1 + \cos\left(\alpha_1 + \arctan\frac{k_x}{k_z}\right)\right) \quad (34)$$

where L_1 is the distance between the gratings along the normal, $k_{zx}^2 = \left(\frac{\omega}{c}\right)^2 - k_y^2$, and θ is found from the grating equation:

$$\sin\theta_1\left(\omega,k_x\right) = m\frac{2\pi}{k_{zx}(\omega)}N_1 + \sin\left(\alpha_1 + \arctan\frac{k_x}{k_z(\omega)}\right). \quad (35)$$

The choice of the position of points A1 and C1 on the z-axis is arbitrary, but it is important that they should have the same coordinates on the z-axis, that is, C1 must be strictly above A1. The expression in Equation (34) was derived in the classical work by Treacy[27] in other notation. Note that sometimes (see, e.g., Ref. [25]), instead of Equation (34) it is assumed that $\Psi_1 = \frac{\omega}{c}p$, where p is the path length from A1 to C1, which contradicts Equation (34). Taking into account that $k_{zx} \approx \frac{\omega}{c}\left(1 - \frac{k_y^2}{2(\omega/c)^2}\right)$ from Equations (34) and (35) to an accuracy of $k_{x,y}^3$, we obtain the following:

$$\Psi_1\left(\omega,k_x,k_y\right) = L_1\frac{\omega}{c}\left(\cos\theta_1 + \cos\left(\alpha_1 + \frac{k_xc}{\omega}\right)\right) - L_1\frac{c}{2\omega}k_y^2\left(\cos\left(\theta_1\left(k_{x,y}=0\right)\right) + \cos\alpha_1\right), \quad (36)$$

$$\sin\theta_1\left(\omega,k_x,k_y\right) = m\frac{2\pi c}{\omega}N_1\left(1 + \frac{c^2}{2\omega^2}k_y^2\right) + \sin\left(\alpha_1 + \frac{k_xc}{\omega}\right). \quad (37)$$

The second pair of gratings from point A2 to point C2 is equivalent to the first pair from point A1 to C1 accurate

to the replacement of $\Delta\alpha$ by $-\Delta\alpha$ or k_x by $-k_x$, since for $\Delta\alpha > 0, \alpha_1$ increases but α_2 decreases, which is well-described in Figure 1. In other words, the x-axis changes the direction (the x-axis is always directed outward from the grating, rather than inward), and the vector k_x does not change direction, as the gratings are parallel. Thus, from point A2 to point C2, there is spectral phase incursion $\Psi_2 = \Psi_1(-k_x)$, with all subscripts '1' in the expression for Ψ_1 (Equation (36)) replaced by '2'.

During pulse propagation from the input point D1 to the output point D2 the phase incursion is $\Psi = \Psi_1 + \Psi_2 + \Psi_f$, where Ψ_f is the phase incursion in free space of length L_f:

$$\Psi_f(\omega, k_x, k_y) = L_f \frac{\omega}{c} - L_f \frac{c}{2\omega}\left(k_x^2 + k_y^2\right), \qquad (38)$$

where $L_f = |D1A1| + |C1A2| + |C2D2|$. As seen from Figure 1, L_f is the distance between the input and output planes of the compressor. The choice of these planes is arbitrary but it is important that the distance between them is L_f. Finally, from Equations (36)–(38) we obtain the following expressions (Equations (5) and (6)):

$$\begin{aligned}
\Psi(\omega, k_x, k_y) = &\, L_1 \frac{\omega}{c}\left(\cos\theta_1 + \cos\left(\alpha_1 + \frac{k_x c}{\omega}\right)\right) \\
&+ L_2 \frac{\omega}{c}\left(\cos\theta_2 + \cos\left(\alpha_2 - \frac{k_x c}{\omega}\right)\right) \\
&+ L_f \frac{\omega}{c} - \frac{c}{2\omega}k_x^2 L_f - \frac{c}{2\omega}k_y^2\Big(L_f \\
&+ \left(\cos\left(\theta_1\left(k_{x,y} = 0\right)\right) + \cos\alpha_1\right)L_1 \\
&+ \left(\cos\left(\theta_2\left(k_{x,y} = 0\right)\right) + \cos\alpha_2\right)L_2\Big),
\end{aligned}$$

$$\begin{aligned}
\sin\theta_{1,2}(\omega, k_x, k_y) = &\, m\frac{2\pi c}{\omega}N_{1,2}\left(1 + \frac{c^2}{2\omega^2}k_y^2\right) \\
&+ \sin\left(\alpha_{1,2} \pm \frac{k_x c}{\omega}\right).
\end{aligned}$$

Acknowledgement

References

1. C. Danson, J. Bromage, T. Butcher, J.-C. Chanteloup, E. Chowdhury, A. Galvanauskas, L. Gizzi, C. Haefner, J. Hein, D. Hillier, N. Hopps, Y. Kato, E. Khazanov, R. Kodama, G. Korn, R. Li, Y. Li, J. Limpert, J. Ma, C. H. Nam, D. Neely, D. Papadopoulos, R. Penman, L. Qian, J. Rocca, A. Shaykin, C. Siders, C. Spindloe, S. Szatmári, R. Trines, J. Zhu, P. Zhu, and J. Zuegel, High Power Laser Sci. Eng. **7**, e54 (2019).

2. V. I. Bespalov and V. I. Talanov, J. Exp. Theor. Phys. Lett. **3**, 307 (1966).

3. S. Y. Mironov, V. V. Lozhkarev, V. N. Ginzburg, I. V. Yakovlev, G. Luchinin, A. A. Shaykin, E. A. Khazanov, A. A. Babin, E. Novikov, S. Fadeev, A. M. Sergeev, and G. A. Mourou, IEEE J. Select. Top. Quantum Electron. **18**, 7 (2012).

4. E. A. Khazanov, S. Y. Mironov, and G. Mourou, Phys.-Usp. **62**, 1096 (2019).

5. E. A. Khazanov, Quantum Electron. **52**, 208 (2022).

6. Y. Peng, Y. Xu, and L. Yu, Reza Kenkyu **49**, 93 (2021).

7. X. Wang, X. Liu, X. Lu, J. Chen, Y. Long, W. Li, H. Chen, X. Chen, P. Bai, Y. Li, Y. Peng, Y. Liu, F. Wu, C. Wang, Z. Li, Y. Xu, X. Liang, Y. Leng, and R. Li, Ultrafast Sci. **2022**, 9894358 (2022).

8. J. Bromage, S.-W. Bahk, I. A. Begishev, C. Dorrer, M. J. Guardalben, B. N. Hoffman, J. B. Oliver, R. G. Roides, E. M. Schiesser, M. J. ShoupIII, M. Spilatro, B. Webb, D. Weiner, and J. D. Zuegel, High Power Laser Sci. Eng. **7**, e4 (2019).

9. J. Bromage, S.-W. Bahk, M. Bedzyk, I. A. Begishev, S. Bucht, C. Dorrer, C. Feng, C. Jeon, C. Mileham, R. G. Roides, K. Shaughnessy, M. J. Shoup III, M. Spilatro, B. Webb, D. Weiner, and J. D. Zuegel, High Power Laser Sci. Eng. **9**, e63 (2021).

10. J. Kawanaka, K. Tsubakimoto, H. Yoshida, K. Fujioka, Y. Fujimoto, S. Tokita, T. Jitsuno, N. Miyanaga, and G.-E. D. Team, J. Phys. Conf. Ser. **688**, 012044 (2016).

11. Z. Li and J. Kawanaka, Rev. Laser Eng. **49**, 101 (2021).

12. Z. Li, Y. Kato, and J. Kawanaka, Sci. Rep. **11**, 151 (2021).

13. E. Khazanov, A. Shaykin, I. Kostyukov, V. Ginzburg, I. Mukhin, I. Yakovlev, A. Soloviev, I. Kuznetsov, S. Mironov, A. Korzhimanov, D. Bulanov, I. Shaikin, A. Kochetkov, A. Kuzmin, M. Martyanov, V. Lozhkarev, M. Starodubtsev, A. Litvak, and A. Sergeev, High Power Laser Sci. Eng. **11**, e78 (2023).

14. Z. Li, Y. Leng, and R. Li, Laser & Photonics Rev. **17**, 2100705 (2022).

15. N. Bonod and J. Neauport, Adv. Opt. Photonics **8**, 156 (2016).

16. J. Liu, X. Shen, S. Du, and R. Li, Opt. Express **29**, 17140 (2021).

17. A. Kochetkov, E. Kocharovskaya, and E. Khazanov, J. Opt. Soc. Am. B **40**, 2851 (2023).

18. S. Mironov, V. Lozhkarev, G. Luchinin, A. Shaykin, and E. Khazanov, Appl. Phys. B Lasers Opt. **113**, 147 (2013).

19. V. N. Ginzburg, A. A. Kochetkov, A. K. Potemkin, and E. A. Khazanov, Quantum Electron. **48**, 325 (2018).

20. O. Shorokhov, A. Pukhov, and I. Kostyukov, Phys. Rev. Lett. **91**, 265002 (2003).

21. M. Martyanov and E. Khazanov, J. Opt. Soc. Am. A **40**, 1507 (2023).

22. A. Kochetkov, M. Martyanov, V. Ginzburg, and E. Khazanov, Laser Phys. Lett. **20**, 065001 (2023).

23. S. Du, X. Shen, W. Liang, P. Wang, and J. Liu, Photonics **9**, 445 (2022).

24. X. Shen, S. Du, W. Liang, P. Wang, J. Liu, and R. Li, Appl. Phys. B **128**, 159 (2022).

25. S. Du, X. Shen, W. Liang, P. Wang, J. Liu, and R. Li, High Power Laser Sci. Eng. **11**, e4 (2023).

26. Z. Li, J. Liu, Y. Xu, Y. Leng, and R. Li, Opt. Express **30**, 41296 (2022).

27. E. B. Treacy, IEEE J. Quantum Electron. **QE-5**, 454 (1969).

28. W. H. Williams, J. K. Crane, D. A. Alessi, C. D. Boley, M. W. Bowers, A. D. Conder, J.-M. G. D. Nicola, P. D. Nicola, C. Haefner, J. M. Halpin, M. Y. Hamamoto, J. E. Heebner, M. R. Hermann, S. I. Herriot, D. C. Homoelle, D. H. Kalantar, T. E. Lanier, K. N. LaFortune, J. K. Lawson, R. R. Lowe-Webb, F. X. Morrissey, H. Nguyen, C. D. Orth, L. J. Pelz, M. A. Prantil,

M. C. Rushford, R. A. Sacks, J. T. Salmon, L. G. Seppala, M. J. Shaw, R. J. Sigurdsson, P. J. Wegner, C. C. Widmayer, S. T. Yang, and T. L. Zobrist, Appl. Opt. **60**, 2288 (2021).

29. J. K. Crane, G. Tietbohl, P. Arnold, E. S. Bliss, C. Boley, G. Britten, G. Brunton, W. Clark, J. W. Dawson, S. Fochs, R. Hackel, C. Haefner, J. Halpin, J. Heebner, M. Henesian, M. Hermann, J. Hernandez, V. Kanz, B. McHale, J. B. McLeod, H. Nguyen, H. Phan, M. Rushford, B. Shaw, M. Shverdin, R. Sigurdsson, R. Speck, C. Stolz, D. Trummer, J. Wolfe, J. N. Wong, G. C. Siders, and C. P. J. Barty, J. Phys. Conf. Ser. **244**, 032003 (2010).

30. J. E. Harvey, S. Schröder, N. Choi, and A. Duparré, Opt. Eng. **51**, 013402 (2012).

31. V. E. Asadchikov, I. V. Kozhevnikov, Y. S. Krivonosov, R. Mercier, T. H. Metzger, C. Morawe, and E. Ziegler, Nucl. Instrum. Methods Phys. Res. A **530**, 575 (2004).